Engineering Structures 73 (2014) 54–61

Contents lists available at ScienceDirect

Engineering Structures

journal homepage: www.elsevier.com/locate/engstruct

The impact of passive tuned mass dampers and wind–wave misalignment on offshore wind turbine loads

Gordon M. Stewart, Matthew A. Lackner *

Department of Mechanical and Industrial Engineering, University of Massachusetts Amherst, 160 Governors Drive, Amherst, MA 01003, USA

ARTICLE INFO

Article history:
Received 14 October 2013
Revised 18 April 2014
Accepted 25 April 2014

Keywords:
Structural control
Wind turbine
Passive
Offshore
Wave misalignment
Loads

ABSTRACT

Offshore wind turbines experience complex external loading from a variety of sources, especially wind and waves. To be economical, offshore wind turbine must operate reliably under these loading conditions. The external loading is complicated by the directionality of the wind and the waves. Metocean data in Europe and the US shows that the wind and the waves are often misaligned by significant amounts. This misalignment causes large loads on the tower in the side-side direction, which has very little structural damping compared to the fore-aft direction. Recent papers have highlighted the importance of considering wind–wave misalignment when analyzing the loads of offshore wind turbines. A variety of approaches are feasible and have been investigated to mitigate loading on offshore wind turbines due to the wind and waves. Many approaches control the aerodynamic loading on the rotor, either via control of the blade pitch or other aerodynamic actuation. This paper analyzes an alternative approach using structural control, in which passive tuned mass dampers are used to absorb and dissipate structural vibrations. In particular, this study investigates the load mitigation potential of passive tuned-mass-dampers for a 5 MW offshore wind turbine supported by a monopile, and subjected to realistic external conditions that include wind–wave misalignment. A comprehensive set of operational simulations is used to demonstrate that optimally tuned passive tuned-mass-dampers are capable or reducing tower fore-aft and side-side fatigue loads by approximately 5% and 40%, respectively. A discussion of the practical feasibility of such an approach is also provided.

1. Introduction

Offshore wind turbines (OWTs) operating in the marine environment are subjected to external loading from a variety of sources including wind, waves, current, and ice [1–3]. These external loads impact the major components of the OWT and may lead to failures and costly downtime [4–7]. For offshore wind energy to be cost effective, OWTs must be able to withstand these loads and operate reliably. Reliability is particularly crucial for OWTs (in contrast to land-based) because maintenance is expensive, dangerous, and often impossible for prolonged periods when the sea states are sufficiently harsh.

While it is well-known that the loading from wind and waves may eventually cause fatigue or ultimate load failures in OWTs, the majority of simulations and analysis of OWT loads in the literature utilize conditions in which the wind and waves are aligned in the same direction, referred to here as the fore-aft direction [8–12]. Given that wind is a primary driving force for waves, the use of aligned wind and waves appears logical. Some recent studies, however, have demonstrated two important factors: (i) the percentage of time that an OWT operates with misaligned wind and waves is significant; and (ii) because OWTs have very little structural damping in the side-side direction, which is orthogonal to the aerodynamic damping provided by the rotor thrust in the fore-aft direction, misaligned waves increase the overall loading on the support structure [13,14]. For example, a wind–wave misalignment of 90° was shown to increase the side-side mud-line bending moment by a factor of 5, while the fore-aft mud-line bending moment only decreased by 30%. On an absolute scale the side-side mud-line bending moment for 90° misalignment was approximately 25% greater than the fore-aft mud-line bending moment for a standard 0° misalignment [13].

The motivation to reduce loads on OWTs and improve reliability is compelling, and numerous load mitigation approaches have been evaluated for both fixed-bottom and floating turbines, including individual pitch control [8,12,15], acceleration feedback control [16–19], active generator torque control [20,19] feed-forward control using lidars [21], and smart rotors with active aerodynamic devices [22,23]. These approaches all focus on controlling the

* Corresponding author.
E-mail addresses: gmstewar@student.umass.edu (G.M. Stewart), lackner@ecs.umass.edu (M.A. Lackner).

http://dx.doi.org/10.1016/j.engstruct.2014.04.045
0141-0296/

aerodynamic loading on the blades. An alternative approach to reduce the loads on OWTs is structural control, which affects the response of the structure itself, and is the focus of this paper. The control of civil engineering structures has been an active research area for over two decades, with the goal of protecting structures from dynamic loading due to earthquakes, wind, waves, and other sources [24–30]. There are three major categories of control methods for structures: passive, semi-active, and active [25]. Passive structural control techniques are the most straightforward, with constant parameters and no energy input, and are the focus of this paper. A simple example of a passive system is a mass-spring-damper (“tuned mass damper” or TMD) that is tuned to absorb energy at one of the natural frequencies of the main structure [27]. A wide range of potential passive actuators exist for structural control, including tuned mass dampers, tuned sloshing dampers, tuned liquid dampers, tuned liquid column dampers, friction dampers, pendulum dampers, and more [24,31–36]. The investigations carried out in this research use a TMD, although other passive actuators can me modeled as a TMD, making the results fairly general.

Early research on structural control of OWTs, excluding that of the authors and collaborators, has focused on passive control of fixed bottom OWTs using relatively simple, limited degree of freedom models that lack detailed modeling of the metocean conditions and resulting stochastic loads on the structure [34,37–40]. In the previous work of the authors and collaborators, a much higher fidelity modeling tool was developed, FAST-SC, which is an extended version of the aero-elastic design code FAST and is discussed in more detail in Section 2 [41]. Using FAST-SC, passive and active systems were designed, optimized, and evaluated for fixed-bottom and floating OWTs under realistic stochastic external loading conditions, but with aligned wind and waves only [42–45]. For an OWT with a monopile support structure with aligned wind and waves, two passive TMDs of approximately 2% of the total system mass, with one TMD oscillating in the fore-aft direction and the other side-side, reduced fore-aft and side-side fatigue loads by 7% and 60%, respectively [44]. The minimal damping in the side-side direction is obvious from these results as the addition of a TMD that oscillates in the side-side direction produces very large load reductions. For a floating barge OWT, passive and active structural control are able to reduce fatigue loads by approximately 10% and 25%, respectively, depending on the active control authority and thus power consumption [42,43,45].

The goal of the research presented in this paper is to evaluate passive structural control applied to an OWT monopile in the presence of wind–wave misalignment. wind–wave misalignment has traditionally been ignored in OWT loads analysis, but the effect of misalignment on loads is significant, and this investigation is the first to consider the combined effects of passive structural control and wind–wave misalignment. The impact of wind–wave misalignment on the loads of a baseline 5 MW OWT monopile is determined, and then the load reductions due to passive TMDs of varying mass and orientation within the nacelle are quantified. The results demonstrate that passive TMDs are an effective load mitigation strategy for OWT monopiles, and in particular are capable of reducing side-side loads in the presence of wind–wave misalignment. While this paper does not investigate detailed design of a passive system and instead considers a generic TMD, a brief discussion of the feasibility of such a system is presented.

2. Simulation tools and turbine models

2.1. FAST with HydroDyn

FAST is a fully coupled aero-hydro-servo-elastic code, developed at the National Renewable Energy Laboratory, that simulates the loads and performance of modern wind turbines [46]. When running a simulation using FAST, the aerodynamics are calculated with the AeroDyn subroutine, which uses the well-known equilibrium Blade Element-Momentum (BEM) approach. The AeroDyn calculations include the effects of axial and tangential induction, tip and hub losses (using the Prandtl model), and the Beddoes–Leishman dynamic stall model.

The structural dynamics are calculated by modeling the blades and tower with a linear modal representation. The blades and tower are modeled as flexible bodies, with distributed mass and stiffness properties, and prescribed mode shapes. There are two flapwise and one edgewise degrees of freedom (DOF) for the blades, and two fore-aft and two side-side DOFs for the tower.

The capability for modeling an offshore floating structure is possible with the HydroDyn subroutine [47]. HydroDyn calculates the hydrodynamic loads on the platform, including hydrostatic restoring contributions of buoyancy and waterplane area, viscous drag calculated using Morisons equation, added mass and damping contributions from wave radiation, including free surface memory effects, and the incident wave excitation from scattering in regular or irregular seas [47]. The loads from the mooring system are also calculated.

FAST uses a time marching simulation to solve the non-linear equations of motion of the fully coupled model. A schematic detailing the various modules in FAST is shown in Fig. 1.

2.2. Description of FAST-SC

Previous publications describe the theoretical background and practical implementation for modeling structural control in FAST, which resulted in the “FAST-SC” code [41,42]. Details are available in these earlier publications, and a brief summary is provided here. FAST-SC can model two independent TMDs with a user-defined mass, spring stiffness, damping, and translation direction. Earlier investigations defined the TMDs as translating in the fore-aft and side-side directions exclusively, but any arbitrary rotation of the TMD translation direction about the vertical axis is possible. An example of a fore-aft oriented TMD is shown in Fig. 2. The TMDs can be located in the nacelle or the platform, which is useful in the case of floating OWTs. While this paper investigates passive control, the code can run with the FAST-Simulink interface for semi-active and active control, with the spring stiffness, damping, and external force input for each TMD commanded in Simulink.

2.3. NREL 5 MW turbine and monopile models

The wind turbine model used for the analysis in FAST is the NREL 5 MW wind turbine [49]. This turbine model is widely used by many other researchers to evaluate offshore wind turbine loads and control strategies. The main features of the NREL 5 MW model are shown in Table 1. The support structure is designed for 20 m water depth.

2.4. Tuned mass damper parameters and configurations

Previous work by the authors describes the procedure for determining optimal TMD properties for an OWT monopile [44]. Specifically, the procedure determined the optimal spring stiffness and damping values for two values of the TMD mass, 10,000 kg and 20,000 kg. The optimal parameters are shown in Table 2. The damped natural frequency of the TMDs is similar to the first natural frequency of the tower, which is 0.31 Hz for the NREL 5 MW supported by a monopile, indicating that the optimization procedure tunes the TMD to this particular structural mode. These parameters are optimal for both a fore-aft and side-side translating TMD, and a sensitivity analysis indicated that the load reductions

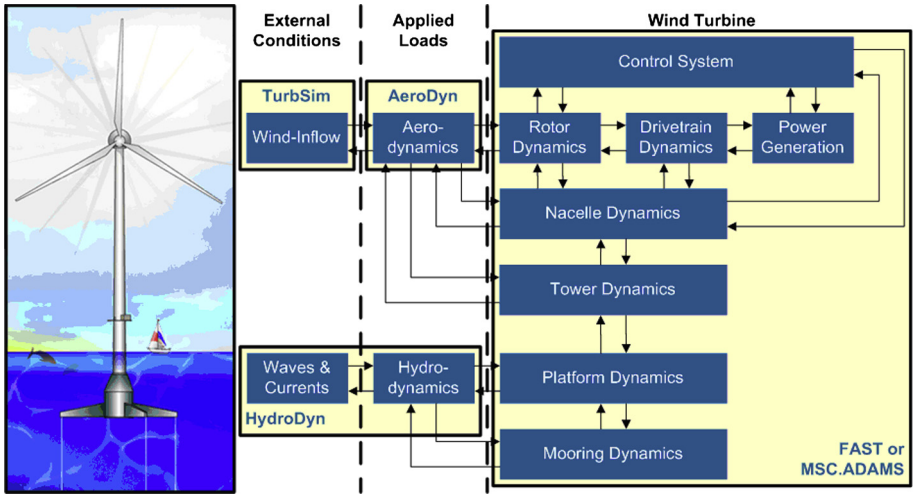

Fig. 1. Schematic of FAST modules [48].

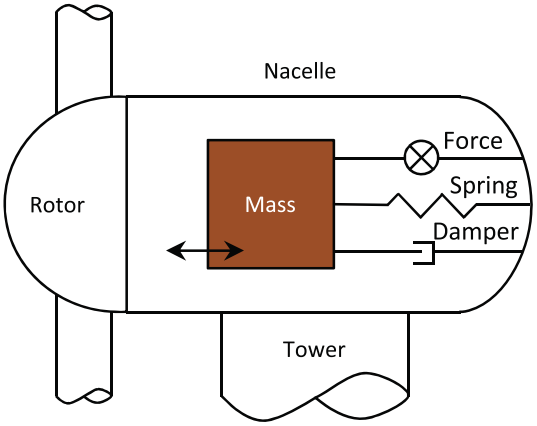

Fig. 2. Schematic of a fore-aft TMD in the nacelle.

Table 1
Physical parameters of NREL 5 MW baseline turbine [49].

Rating	5 MW
Rotor Orientation, Configuration	Upwind, 3 Blades
Control	Variable Speed, Collective Pitch
Drivetrain	High Speed, Multiple-Stage Gearbox
Rotor, Hub Diameter	126 m, 3 m
Hub Height	90 m
Cut-In, Rated, Cut-Out Wind Speed	3 m/s, 11.4 m/s, 25 m/s
Cut-In, Rated Rotor Speed	6.9 rpm, 12.1 rpm
Rated Tip Speed	80 m/s
Overhang, Shaft Tilt, Precone	5 m, 5°, 2.5°
Rotor Mass	110,000 kg
Nacelle Mass	240,000 kg
Tower and Monopile Mass	522,617 kg
Nacelle Dimensions	18 m × 6 m × 6 m

Table 2
Optimal TMD parameters for the NREL 5 MW supported by a monopile.

Mass (kg)	k (N/m)	d (N/(m/s))	ω_n (Hz)	ω_d (Hz)	ζ (%)
10,000	28,805	2800	0.270	0.269	8.3
20,000	54,274	7414	0.262	0.259	11.3

are insensitive to variations of the optimal parameters on the order of 5–10%.

As discussed above, the translation directions of the TMDs can be specified. In this paper, two translation direction configurations are evaluated. In the first configuration, one TMD mass translates in the fore-aft direction and the other in the side-side, forming a "+" and referred to as the 0° configuration. In the other configuration, the translation direction of each TMD is rotated by 45° about the vertical axis, forming an "X" and referred to as the 45° configuration. These two translation direction configurations are evaluated for each TMD mass and associated optimal parameters, for a total of four configurations utilizing TMDs, as well as the baseline configuration with no TMDs.

While the mass of the TMDs may appear large, the total mass of the rotor-nacelle assembly is 350,000 kg for the NREL 5 MW turbine, and the tower and monopile mass is an additional 523,000 kg [49]. The TMD masses are therefore approximately 1–2% of the total mass of the structure, which is consistent with civil engineering applications of passive structural control. As a point of comparison, a concrete TMD with a 10,000 kg mass has a volume equal to only 0.64% of the total nacelle volume. A system that utilizes water, such as a tuned liquid column damper, has a volume equal to 1.54% of the total nacelle volume.

3. Metocean conditions and simulation parameters

Realistic metocean conditions describing the wind and wave conditions are necessary to obtain probability density functions that can be used to determine fatigue loads. For this study, data from the National Oceanic and Atmospheric Administration (NOAA) offshore floating buoys are used. Historical data from the Long Island buoy site (Station 44025) are used due to this site's proximity to proposed offshore wind sites, long history of data (21 years of data are used in this study), and significant wind–wave misalignment. See Fig. 3 for the location of this site. Section 3.1 describes the procedure for developing the joint probability density functions (PDFs) used to weight the results of the simulations.

3.1. Characterization of metocean conditions

The raw data from the Long Island site are downloaded from the National Data Buoy Center website (www.ndbc.noaa.gov). Sensor malfunctions and other errors in data collection are somewhat common in these data files, so these errors are removed from the raw data. The output channels of wind speed, significant wave height, wave peak spectral period, wind direction and wave direction are used to establish the input conditions for the

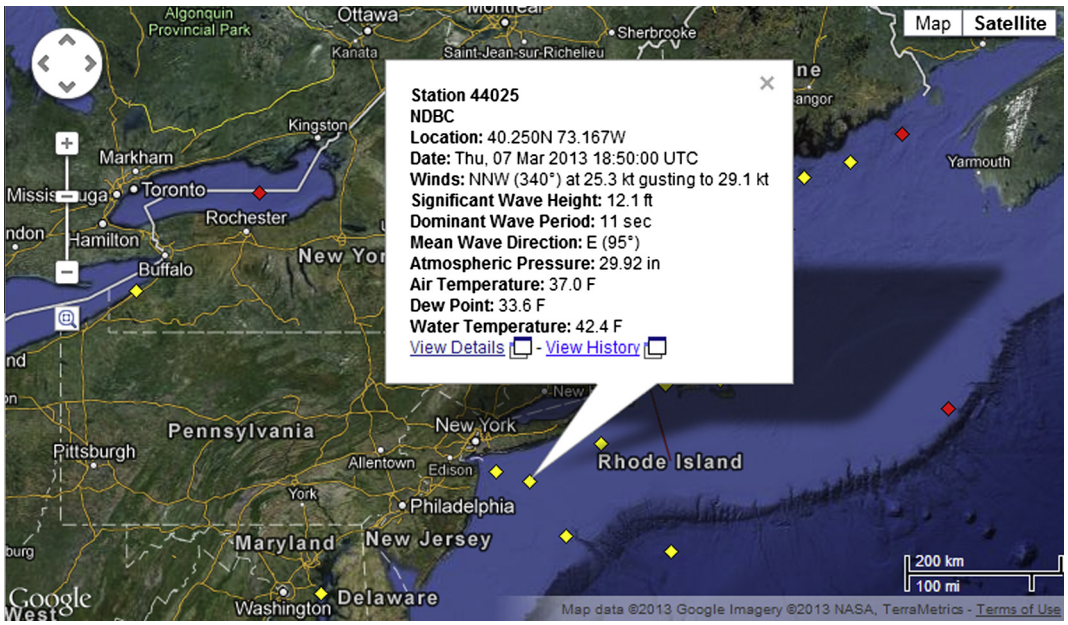

Fig. 3. Location of Station 44025 data buoy.

simulations. The difference between the wind and wave directions is found using a modulo operation to create a wind–wave misalignment angle, β, such that: $-180^\circ \leqslant \beta < 180^\circ$. A wind shear power law with an exponent of 0.1 is used to extrapolate the wind speed from the sensor height of 5 m to the hub height of 90 m.

The data are then binned by the mean wind speed, $\overline{U}$, and β. The bins for $\overline{U}$ are 2 m/s wide, from the cut-in wind speed of 3 m/s to the cut-out wind speed of 25 m/s, for 11 total bins. Wind–wave misalignment angle is divided into 24 bins with 15° width. In this study, $\overline{U}$ and β are the two independent input parameters, resulting in a total of 264 independent bins. Next, the expected values for significant wave height and peak spectral period are calculated. The significant wave height is conditioned on $\overline{U}$ and β, so for each of $\overline{U}$ and β bins, the average significant wave height is calculated, shown in Fig. 4. The peak spectral period is conditioned on $\overline{U}$ and significant wave height. The resulting surface is interpolated to the β bins and shown in Fig. 4. Note that large values of β are rare, and so some noise appears in the surface plots shown in Fig. 4 at these large values of β.

Joint PDFs are then fit to the binned data. First a two-parameter Weibull distribution is fit to the mean wind speed data. Next, a Von Mises distribution is fit to the misalignment values in each mean wind speed bin. The Von Mises distribution is also known as the circular normal distribution, and approximates a Gaussian distribution that is mapped to a circular domain. Once these distributions are fit to the data, the joint probability can be computed as seen in Eq. (1), where P is the probability of a given mean wind speed $\overline{U}$ and wind–wave misalignment β, β_L and β_H are the lower and upper limits of the misalignment bin, $\overline{U}_L$ and $\overline{U}_H$ are the lower and upper limits of the wind speed bin, F_β and $F_{\overline{U}}$ are the cumulative distribution functions of the misalignment and wind speed, and λ and k are the scale and shape parameters of the 2 parameter Weibull distribution. Note that the parameters of the Von Mises distribution, μ and κ, depend on the mean wind speed bin. A surface plot of the resulting two-dimensional joint PDF can be seen in Fig. 5

$$P(\beta_L < \beta < \beta_H)|(\overline{U}_L < \overline{U} < \overline{U}_H) = [F_\beta(\beta_H; \mu(\overline{U}), \kappa(\overline{U})) - F_\beta(\beta_L; \mu(\overline{U}), \kappa(\overline{U}))] \times [F_{\overline{U}}(\overline{U}_H; \lambda, k) - F_{\overline{U}}(\overline{U}_L; \lambda, k)] \quad (1)$$

3.2. Simulation parameters

A series of time domain simulations are performed to evaluate the impact of passive TMDs in the presence of wind–wave misalignment. The simulation conditions are based on the International Electrotechnical Commission (IEC) "61400-3 Design Requirements for Offshore Wind Turbines," specifically design load case (DLC) 1.2. A summary of the simulation conditions and TMD configurations is given below:

- The NREL 5 MW turbine with a monopile in 20 m water depth is modeled in FAST-SC, and all relevant DOFs are enabled, including all of the blade and tower structural DOFs, and the generator and yaw DOFs [46].
- Five configurations are evaluated, the baseline design with no TMD and the four TMD configurations discussed in Section 2.4.
- As discussed in Section 3.1, the metocean data is broken up into 24 15° wind–wave misalignment bins and 11 mean wind speed bins. For each of the 264 total bins, the probability of occurrence, expected value of the significant wave height, and expected value of the peak spectral period are defined.
- For each bin, six simulations with 600 s of usable data per simulation are conducted, for a total of 1584 simulations for a given configuration and 7920 total. Each simulation uses a stochastic 3D turbulent wind file with a different random seed generated using TurbSim [50], each with the associated mean wind speed for the bin. The normal turbulence model (NTM) and the von Karman spectrum are used. Likewise, each simulation uses the Jonswap spectrum and a different random seed to generate the stochastic waves with the associated wave properties for the bin.
- The following output channels are considered: flapwise and edgewise blade bending moments, and tower base fore-aft and side-side bending moments.
- For each output channel, the NREL program MLife is utilized to calculate fatigue loads, specifically the fatigue damage equivalent loads (DELs) [51,52]. The standard version of MLife uses a Weibull distribution for the wind speed to

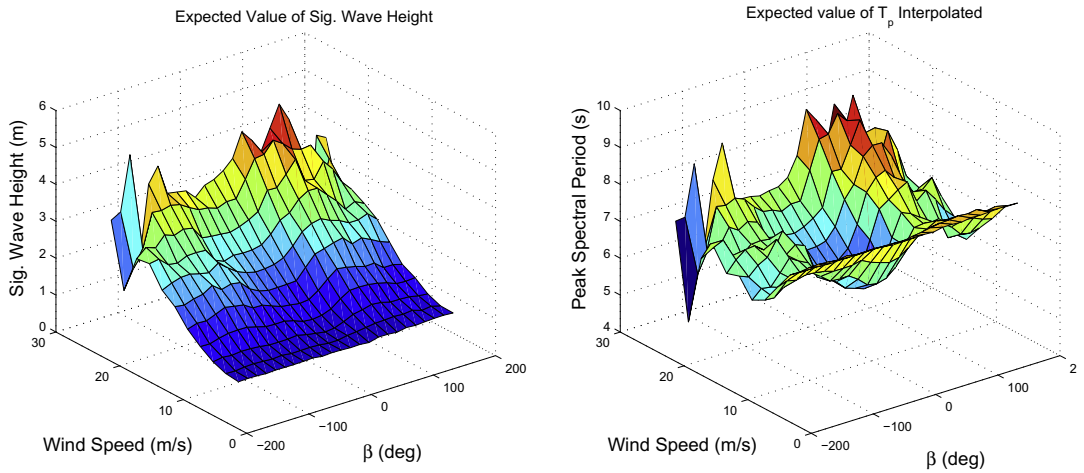

Fig. 4. Expected value of significant wave height (left) and peak spectral period (right) as a function of the mean wind speed and misalignment angle.

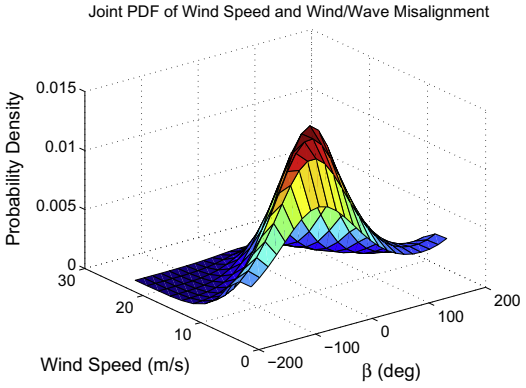

Fig. 5. Joint probability density function of mean wind speed and wind/wave misalignment.

weight the loads in order to estimate lifetime fatigue DELs. Due to the use of a joint PDF of mean wind speed and wind–wave misalignment, a modified version of MLife is used that can be supplied with a user-defined n-dimensional probability function (see Section 3.1). MLife uses a rainflow counting algorithm to determine the cycle counts at various load ranges, and then uses Miner's rule to sum the load cycles in each bin, producing short-term fatigue DELs estimates for each simulation condition. Finally, the joint PDF of the mean wind speed and wind–wave misalignment is used to create a weighted sum of the short-term fatigue DELs in every bin, yielding overall fatigue DELs values across all simulations for a given configuration.

4. Results and analysis

4.1. Baseline loads

Fig. 6 shows the baseline fore-aft and side-side tower DELs surface, the mean wind speed and the wind–wave misalignment joint PDF (Fig. 5), and the convolution of the two surfaces. Tower fore-aft DELs (left, first row) increase with increasing mean wind speed, due to increasing rotor thrust up until the rated wind speed of 11.4 m/s as well as the increasing significant wave height as mean

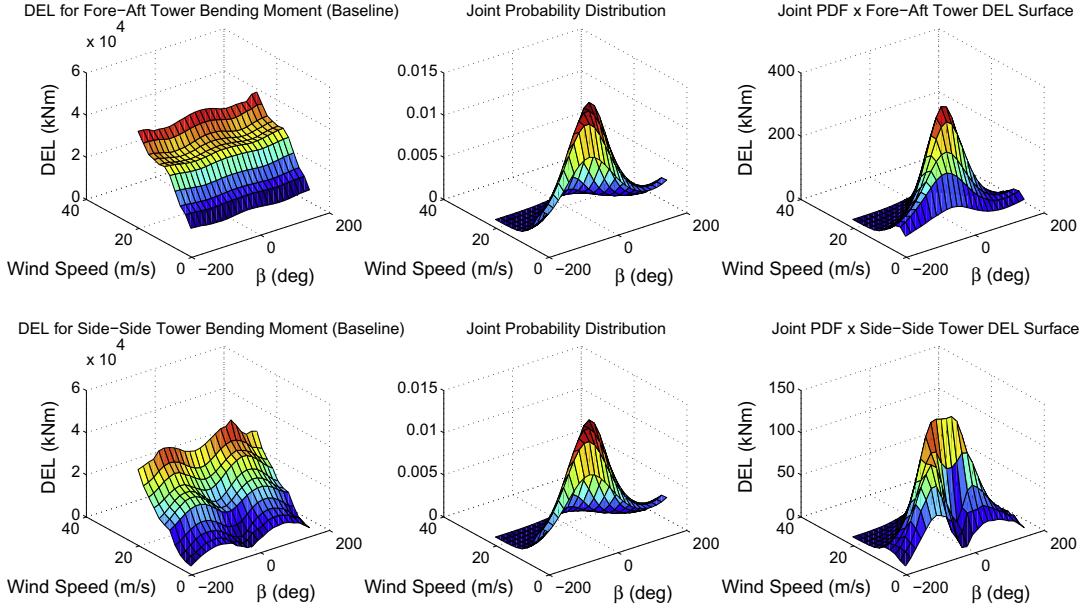

Fig. 6. Baseline fore-aft (top) and side-side (bottom) tower load surfaces (left), mean wind speed/misalignment joint PDFs (center), and convolutions (right).

Table 3
Weighted lifetime tower DEL comparison for all simulations.

	Tower fore-aft damage (kN m)	Improvement from baseline (%)	Tower side-side damage (kN m)	Improvement from baseline (%)
Baseline	30,664	–	24,518	–
10,000 kg, 0°	29,361	4.25	14,321	41.59
10,000 kg, 45°	29,361	4.25	14,318	41.60
20,000 kg, 0°	28,872	5.85	13,717	44.06
20,000 kg, 45°	28,870	5.85	13,717	44.05

wind speed increases (shown in Fig. 4). The fore-aft loads are fairly insensitive to β but are slightly larger for β values near 0°. Tower side-side DELs (left, second row) also increase with increasing $\overline{U}$, but are much more dependent on β than the fore-aft loads. Specifically, side-side loads are maximized at β values near ±90°, which is consistent with the results of other investigations [13].

When the load surface plots are convolved with the mean wind speed and the wind–wave misalignment joint PDF, the overall contribution to the fatigue is obtained, shown in the plots on the right in Fig. 6. The overall contribution to the baseline loads is largest near the rated wind speed of 11.4 m/s, which is a combined effect of the maximum aerodynamic loads at rated wind speed, and the low probability of higher mean wind speeds and thus large wave heights. Both the fore-aft and especially the side-side loads experience significant loading at β values far from 0°, highlighting how critical it is to consider the effect of wind–wave misalignment.

4.2. The impact of TMDs on loads

Table 3 shows the processed results of all simulations, in particular the total (DELs) for each configuration for the tower output channels, weighted by the joint PDFs discussed above. For the baseline tower loads, the fore-aft loads are larger than the side-side loads, but because the analysis includes the wind–wave misalignment, the side-side loads are also significant. These results once again indicate the importance of considering wind–wave misalignment, as simulations of only aligned wind and waves would have much lower side-side loads. The blade loads are not shown in Table 3 because the difference between the baseline and any TMD configuration is less than 1% and deemed negligible. Also, while the TMD displacements are not shown, it should be noted that the maximum displacement across all simulations is less than 0.5 m.

Tables 3 demonstrate that the addition of the TMDs reduces the fore-aft loads by approximately 4–6%, while the side-side loads are reduced by over 40%. The fore-aft motion of the tower is damped by the aerodynamic forces on the rotor, but because there is very little damping in the side-side direction, the addition of the TMDs has a much larger effect on the side-side loads. The results also show that the load reductions are fairly insensitive to the mass and orientation of the TMDs. The heavier TMDs have larger load reductions, but the marginal improvement from increasing the TMD mass is much smaller than simply including a TMD to begin with. It seems clear that to save cost and space, a smaller TMD is justified.

Time series plots are shown in Fig. 7, which compare the tower base fore-aft and side-side bending moment for the baseline and the 10,000 kg, 0° configurations for two particular simulation conditions – $\overline{U} = 10$ m/s, $\beta = 0°$ and $\beta = 45°$, respectively. These figure show 12 second windows of the total simulations, to enable easier comparison. The effectiveness of the TMDs at reducing the amplitude of the variation of the bending moment is apparent in all plot, but is most significant for the side-side bending moment in the 45° misalignment case.

Fig. 8 shows surface plots of the tower fore-aft DELs for the baseline configuration and one TMD configuration (10,000 kg and 0°), as well as the difference between the two configurations, as a function of $\overline{U}$ and β. The baseline tower fore-aft load surface is discussed above in Section 4.1, and the load surface for this TMD configuration has similar trends and magnitudes. The surface

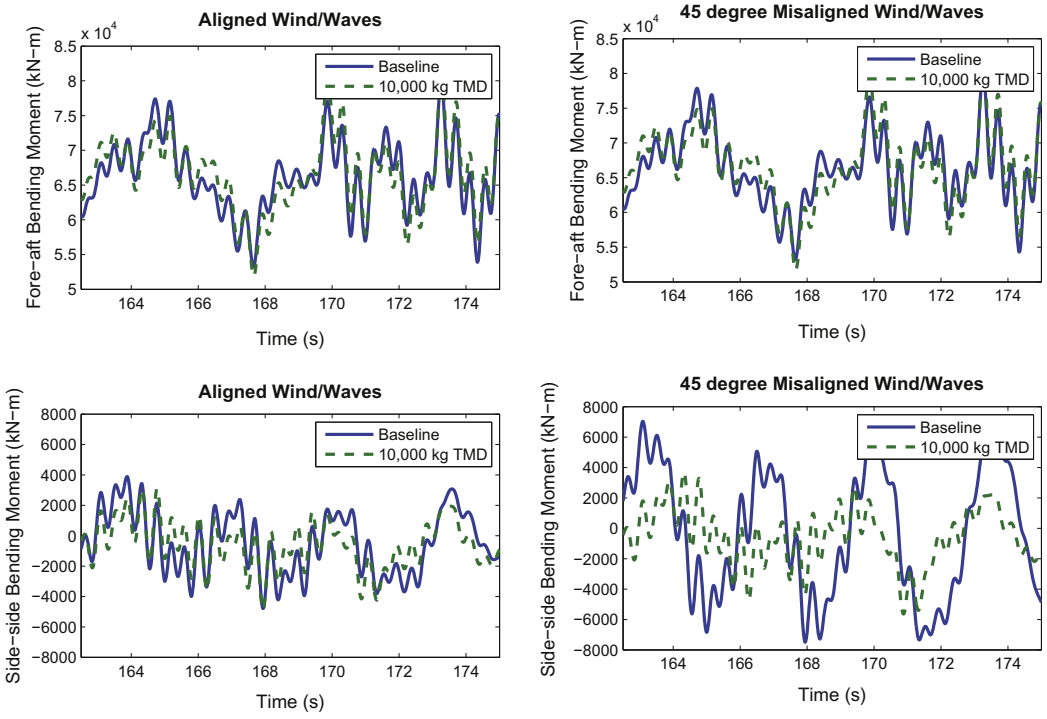

Fig. 7. Tower base bending moments for the baseline case, and 10,000kg, 0° TMD.

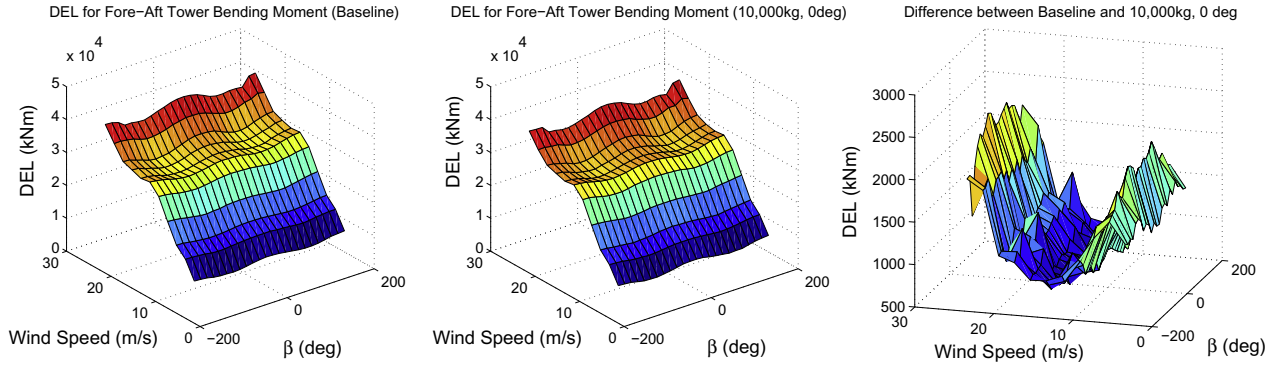

Fig. 8. Fore-aft tower DELs for the baseline case, 10,000kg, 0° TMD, and the difference between baseline and this TMD.

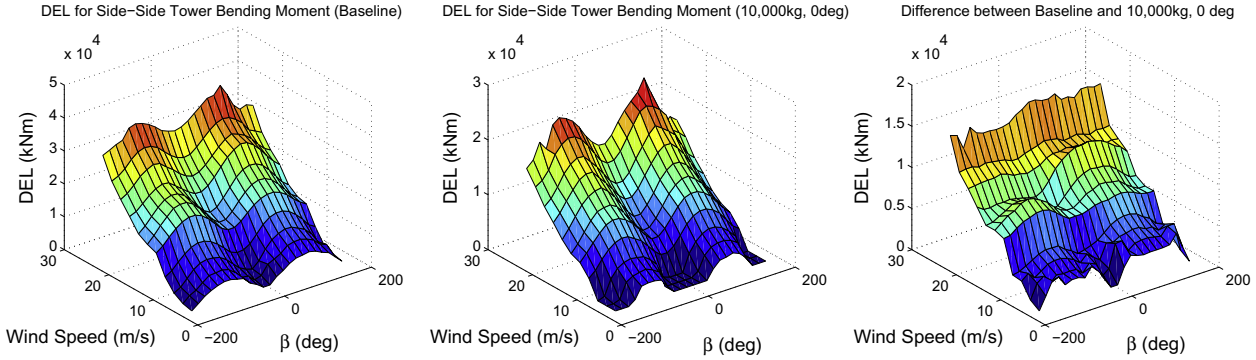

Fig. 9. Side-side tower DELs for the baseline case, 10,000kg, 0° TMD, and the difference between baseline and this TMD.

showing the difference between the two configurations highlights how the TMD primarily reduces tower fore-aft loads at low and high mean wind speeds, and is least effective near rated wind speed. This result seems logical, as the rotor thrust and thus the aerodynamic damping is maximum at rated wind speed.

Fig. 9 is identical to Fig. 8 except it shows the tower side-side DELs. The baseline tower side-side load surface is discussed above in Section 4.1, and while the load surface for this TMD configuration has similar trends, notice that the z-axes for the left and center plots are different, indicating the significant decrease in side-side loading when the TMDs are included. The surface showing the difference between the two configurations shows that the TMDs become more effective at β values near $\pm 90^\circ$ and as $\overline{U}$, and so the significant wave height, increases.

5. Conclusions

This paper presents an investigation into the use of passive structural control techniques for offshore wind turbines subjected to realistic external conditions, in particular taking into account the effect of wind–wave misalignment on the tower loads. The comprehensive simulations clearly demonstrate that wind–wave misalignment leads to large side-side tower loads in the baseline case, which are less than but of the same order at the fore-aft loads.

Including optimized TMDs in the FAST-SC simulations shows that the primary impact of the TMDs is on the side-side loads, which are reduced by over 40%, as a result of the minimal structural damping in this direction compared to the aerodynamic damping provided by the rotor in the fore-aft direction. The results also show that there is little benefit in increasing the TMD mass from 10,000 kg to 20,000 kg, and that the orientation of the TMDs does not affect the loads. The insensitivity to orientation, combined with the small displacement of the TMDs, suggests that they could just as effectively be located at the top of the tower rather than in the nacelle, which may be more convenient. Because the TMDs would not yaw with the nacelle, they would essentially experience all orientations, which does not appear to impact the load reductions.

From a practical perspective, passive structural control, and specifically tuned-mass-dampers, are a relatively cheap and robust solution to suppress tower vibrations in the offshore environment, resulting in lower fatigue loads. While utilizing TMDs adds extra mass to the system, it can be "dumb" mass constituted by concrete or even water. TMDs are a relatively new consideration for OWTs, but in many civil engineering application with similar issues related to complex external loading, the beneficial load reductions have been determined to outweigh the additional mass, cost, and complexity of including a TMD. Thus, while the practical design feasibility of adding a TMD system is not the focus of this paper, the significant load reductions demonstrated in this paper highlight the potential of TMDs as an efficient mechanism for increasing offshore wind turbine reliability.

Acknowledgments

This authors would like to thank Dr. Jason Jonkman from the National Renewable Energy Laboratory for his help in developing FAST-SC. We would also like to thank the National Science Foundation IGERT program for funding this Ph.D. research.

References

[1] Jonkman J. Dynamics modeling and loads analysis of an offshore floating wind turbine. Ph.D. thesis. National Renewable Energy Laboratory; 2008.

[2] Agarwal P, Manuel L. Extreme loads for an offshore wind turbine using statistical extrapolation from limited field data. Wind Energy 2008;11:673–84.
[3] Musial W, Ram B. Large-scale offshore wind power in the united states: assessment of opportunities and barriers. Tech rep. NREL/TP-500-40745. U.S. Department of Energy; 2010.
[4] Bossanyi E. Individual blade pitch control for load reduction. Wind Energy 2003;6:119–28.
[5] van Bussel G. Reliability, availability and maintenance aspects of large-scale offshore wind farms, a concepts study. In: MAREC; 2001. p. 119–26.
[6] Echavarria E, Hahn B, Van Bussel G, Tomiyama T. Reliability of wind turbine technology through time. J Sol Energy Eng. 2008;130(3).
[7] Arwade S, Lackner M, Grigoriu M. Probabilistic models for wind turbine and wind farm performance. J Sol Energy Eng 2011;133(4):041006.
[8] Bossanyi E. Further load reductions with individual pitch control. Wind Energy 2005;8(4):481–5.
[9] Agarwal P, Manuel L. Simulation of offshore wind turbine response for long-term extreme load prediction. Eng Struct 2009;31(10):2236–46.
[10] Jonkman J. Dynamics of offshore floating wind turbines?model development and verification. Wind Energy 2009;12:459–92.
[11] Jonkman J, Matha D. Dynamics of offshore floating wind turbines ? Analysis of three concepts. Wind Energy 2011;14(4):557–69.
[12] Namik H, Stol K. Individual blade pitch control of floating wind turbines. Wind Energy 2010;13(1):74–85.
[13] Fischer T, Rainey P, Bossanyi E, Kuhn M. Study on control concepts suitable for mitigation of loads from misaligned wind and waves on offshore wind turbines supported on monopiles. Wind Eng 2011;5:561–74.
[14] Fischer T. Mitigation of aerodynamic and hydrodynamic induced loads of offshore wind turbines. Ph.D. thesis. University of Stutgart; 2012.
[15] Bossanyi E. Controller for 5 mw reference turbine. Tech rep. UpWind. European Union FP6; 2009.
[16] Hansen C. Pitch control systems for the windpact rotor design study. Tech rep. Windward Engineering, LLC; 2001.
[17] Lackner M. Controlling platform motions and reducing blade loads for floating wind turbines. Wind Eng 2009;33(6):541–53.
[18] Lackner M. An investigation of variable power collective pitch control for load mitigation of floating offshore wind turbines. Wind Energy doi:10.1002/we.1502.
[19] Fischer T, de Vries W, Rainey P, Schmidt B, Argyriadis K, Kuhn M. Offshore support structure optimization by means of integrated design and controls. Wind Energy 2012;15:99–117.
[20] Wright AD, Fingersh LJ, Stol KA. Designing and testing controls to mitigate tower dynamic loads in the controls advanced research turbine. In: 45th AIAA aerospace science meeting and exhibit, Reno; 2007.
[21] Laks J, Pao L, Wright A, Kelley N, Jonkman J. Blade pitch control with preview wind measurements. In: 48th AIAA aerospace sciences meeting and exhibit, Orlando, FL USA; 2010.
[22] Lackner M, van Kuik G. A comparison of smart rotor control approaches using trailing edge flaps and individual pitch control. Wind Energy 2009;13(2–3):117–34.
[23] Lackner M, van Kuik G. The performance of wind turbine smart rotor control approaches during extreme loads. J Sol Energy Eng 2010;132(1):011008.
[24] Spencer B, Sain M. Controlling buildings – a new frontier in feedback. Shock Vib Digest 1998;30(4):267–81.
[25] Spencer B, Nagarajaiah S. State of the art of structural control. J Struct Eng 2003;129(7):845–56.
[26] Adeli H, Saleh A. Integrated structural/control optimization of large adaptive/smart structures. Int J Solids Struct 1998;35(28–29):3815–30.
[27] Soong T, Spencer B. Supplemental energy dissipation: state-of-the-art and state-of-the practice. Eng Struct 2002;24:243–59.
[28] Adeli H. Smart structures and building automation in the 21st century. In: The 25th international symposium on automation and robotics in construction; 2008.
[29] Kanegaonkar H. Smart technology systems in offshore structures: status and needs. In: 9th International offshore and polar engineering conference, Brest, France; 1999.
[30] Singh M, Matheu E. Active and semi-active control of structures under seismic excitation. Earthq Eng Struct Dynam 1997;26:193–213.
[31] Symans M, Constantinou M. Semi-active control systems for seismic protection of structures: a state-of-the-art review. Eng Struct 1999;21:469–87.
[32] NI Y, Ying Z, Wang J, Ko J, Spencer B. Stochastic optimal control of wind-excited tall buildings using semi-active MR-TLCDs. Eng Mech 2004;19:269–77.
[33] Gao H, Kwok K. Optimization of tuned liquid column dampers. Eng Struct 1997;19(6):476–86.
[34] Colwell S, Basu B. Tuned liquid column dampers in offshore wind turbines for structural control. Eng Struct 2009;31:358–68.
[35] Lee H, Wong S, Lee R. Response mitigation on the offshore floating platform system with tuned liquid column damper. Ocean Eng 2006;33:1118–42.
[36] Morz A, Karna T. Mitigation of ice loading: feasibility study of semi-active solution. Working paper. VTT Building and Transport; 2005.
[37] Wilmink A, Hengeveld J, Application of tuned liquid column dampers in wind turbines. Tech rep. Netherlands: Mecal Applied Mechanics; 2006.
[38] Murtagh P, Ghosh A, Basu B, Broderick B. Passive control of wind turbine vibrations including blade/tower interaction and rotationally sampled turbulence. Wind Energy 2007;11(4):305–17.
[39] Enevoldsen I. Effects of a vibration mass damper in a wind turbine tower. Mech Struct Mach 1996;24(2):155–87.
[40] Calderon B. Design and optimization of a wind turbine tower by using a damper device. Master's thesis. Stuttgart University; 2009.
[41] Lackner M, Rotea M. Passive structural control of offshore wind turbines. Wind Energy 2011;14(3):373–88.
[42] Lackner M, Rotea M. Structural control of floating wind turbines. Mechatronics 2011;21(4):704–19.
[43] Stewart G, Lackner M. The effect of actuator dynamics on active structural control of offshore wind turbines. Eng Struct 2011;33(5):1807–16.
[44] Stewart G, Lackner M. Optimization of a passive tuned mass damper for reducing loads in offshore wind turbines. IEEE Transactions on Control Systems Technology 2013;21(4):1090–104.
[45] Namik H, Rotea M, Lackner M. Active structural control with actuator dynamics on a floating wind turbine. In: 51st AIAA aerospace science meeting and exhibit, Dallas, TX; 2013.
[46] Jonkman J, Buhl ML. Fast user's guide. Tech rep. NREL/EL-500-38230. Golden, Colorado: National Renewable Energy Laboratory; 2006.
[47] Jonkman J, Sclavounos P. Development of fully coupled aeroelastic and hydrodynamic models for offshore wind turbines. In: 44th AIAA aerospace science meeting and exhibit, Reno, Nevada; 2006.
[48] Jonkman J, Matha D. A quantitative comparison of the responses of three floating platform concepts. In: European offshore wind 2009 conference and exhibition, Stockholm, Sweden; 2009.
[49] Jonkman J, Butterfield S, Musial W, Scott G. Definition of a 5-mw reference wind turbine for offshore system development. TP 500-38060. National Renewable Energy Laboratory; 2008.
[50] Jonkman B, Buhl ML. Turbsim user's guide. Tech rep. NREL/EL-500-36970. Golden, Colorado: National Renewable Energy Laboratory; 2005.
[51] Freebury G, Musial W. Determining equivalent damage loading for full-scale wind turbine blade fatigue tests. In: 19th American society of mechanical engineers (ASME) wind energy symposium; 2000.
[52] Hayman G. Mlife theory manual for version 1.00. Tech rep. National Renewable Energy Laboratory; 2012.